JCI The Journal of Clinical Investigation

Self-associated molecular patterns mediate cancer immune evasion by engaging Siglecs on T cells

Michal A. Stanczak, … , Alfred Zippelius, Heinz Läubli

J Clin Invest. 2018. https://doi.org/10.1172/JCI120612.

Research | In-Press Preview | Immunology | Oncology

Graphical abstract

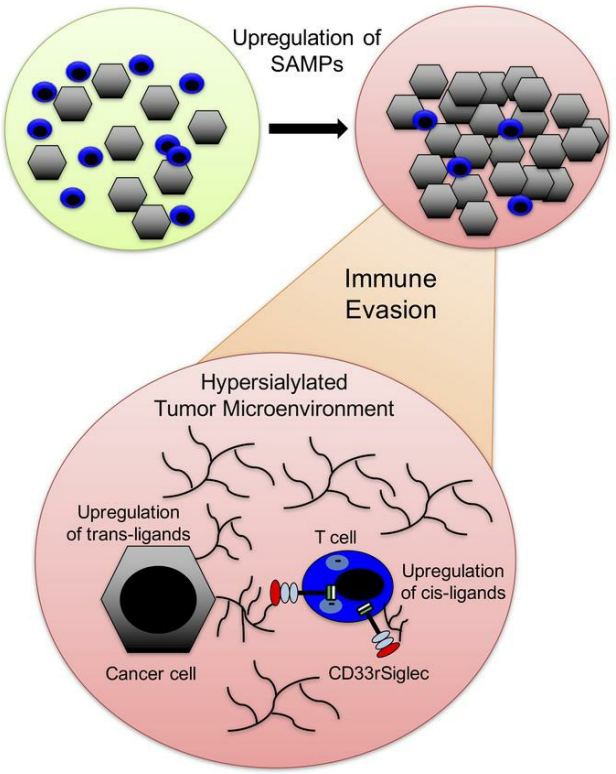

August 12, 2018, Research Article

Self-associated molecular patterns mediate cancer immune evasion by engaging Siglecs on T cells

Michal A. Stanczak[1,2*], Shoib S. Siddiqui[3*], Marcel P. Trefny[1,2], Daniela S. Thommen[1,2], Kayluz Frias Boligan[4], Stephan von Gunten[4], Alexandar Tzankov[5], Lothar Tietze[6], Didier Lardinois[7], Viola Heinzelmann-Schwarz[8], Michael von Bergwelt-Baidon[9], Wu Zhang[10], Heinz-Josef Lenz[10], Younghun Han[11], Christopher I. Amos[11], Mohammedyaseen Syedbasha[12], Adrian Egli[12], Frank Stenner[1,2], Daniel E. Speiser[13], Ajit Varki[3], Alfred Zippelius[1,2] and Heinz Läubli[1,2#]

[1] Cancer Immunology Laboratory, Department of Biomedicine, [2] Division of Oncology, Department of Internal Medicine, University Hospital, Basel, Switzerland, [3] Departments of Medicine and Cellular and Molecular Medicine, Glycobiology Research and Training Center, University of California, San Diego, CA, USA [4] Institute of Pharmacology, University of Bern, Bern, Switzerland, [5] Institute of Pathology, University Hospital Basel, Switzerland, [6]Institute of Pathology, Lahr, Germany, [7]Thoracic Surgery University Hospital, Basel, Switzerland, [8]Gynecological Oncology, University Hospital, Basel, Switzerland, [9]Cologne Interventional Immunology, University of Cologne, Germany, [10]Unversity of Southern California, Los Angeles, CA, USA, [11]Dartmouth College, Hanover, NH, USA, [12]Applied Microbiology Research, University Hospital, Basel, Switzerland, [13]Ludwig Cancer Research Center, University of Lausanne, Switzerland, * these authors contributed equally to this work

[#]Address correspondence to H.L. (heinz.laeubli@unibas.ch), lead contact

Heinz Läubli, Laboratory of Cancer Immunology, Department of Biomedicine, and Medical Oncology, Department of Internal Medicine, University Hospital Basel, Hebelstrasse 20, 4031 Basel, Switzerland, Phone: +41 61 265 5074, Fax: +41 61 265 5316

Keywords: sialic acid, pattern recognition, T cell, tumor immunology, immunotherapy

Abstract

First generation immune checkpoint inhibitors including anti-CTLA-4 and anti-PD-1 antibodies have led to major clinical progress, yet resistance frequently leads to treatment failure. Thus, new targets acting on T cells are needed. CD33-related Siglecs are pattern recognition immune receptors binding to a range of sialoglycan ligands, which appear to function as self-associated molecular patterns (SAMPs) that suppress autoimmune responses. Siglecs are expressed at very low levels on normal T cells, and these receptors were not yet considered as interesting targets on T cells for cancer immunotherapy. Here, we show an upregulation of Siglecs including Siglec-9 on tumor-infiltrating T cells from non-small cell lung cancer (NSCLC), colorectal and ovarian cancer patients. Siglec-9 expressing T cells co-expressed several inhibitory receptors including PD-1. Targeting of the sialoglycan-SAMP/Siglec pathway in vitro and in vivo resulted in increased anti-cancer immunity. T cell expression of Siglec-9 in NSCLC patients correlated with a reduced survival, and Siglec-9 polymorphisms showed associations with the risk of developing lung and colorectal cancer. Our data identify the sialoglycan-SAMP/Siglec pathway as new potential target to improve T cell activation for immunotherapy.

Brief summary

Siglec-9 was identified as a new inhibitory immune checkpoint on tumor-infiltrating $CD8^+$ T cells. Targeting of Siglecs led to an increased anti-tumor activity by T cells.

Introduction

The landscape of oncological practice has significantly changed with the introduction of immune checkpoint inhibitors that target inhibitory receptors on the surface of $CD8^+$ T cells (1). In particular, blocking of the inhibitory receptor programmed death (PD)-1 or its ligand PD-L1 has been shown to induce durable responses across many different cancer types including non-small cell lung cancer (NSCLC), melanoma, squamous carcinoma of the head and neck, kidney cancer or ovarian cancer (1, 2). However, most patients have primary resistance to therapeutic PD-(L)1 blockade or develop secondary resistance (2). Thus, identification of additional pathways mediating suppression of tumor-specific T cells are clearly needed to increase therapeutic efficacy of PD-(L)1 targeting strategies.

Pattern recognition receptors (PRRs) such as Toll-like receptors or nucleotide-binding oligomerization domain (NOD)-like receptors detect pathogens or danger signals and engagement of these PRRs by pathogen-associated molecular patterns (PAMPs) or damage-associated molecular patterns (DAMPs) activate the respective immune cells (3-6). Receptors that bind to PAMPs and DAMPs have also been implicated in cancer progression and anti-cancer immunity (6, 7). In addition to these well-described pathways, sialoglycans have been shown to serve as a 'self-associated molecular patterns' (SAMPs) by binding to CD33-related sialic acid-binding immunoglobulin-like lectins (CD33rSiglecs) (8, 9), a family of receptors on immune cells containing intracellular immunoreceptor tyrosine-based inhibitory motifs (ITIM) (10-13). Unlike the conserved Siglecs (Siglec-1, Siglec-2, Siglec-4 and Siglec-15), CD33rSiglecs including Siglec-3 (CD33), -5, -6, -7, -8, -9, -10, -11, -14 and -16 have evolved rapidly due to multiple selection forces, including evolutionary pressure by pathogens that can mimic sialoglycan-SAMPs (Sia-SAMPs) and bind to inhibitory CD33rSiglecs to escape innate immune control (14-18). The different Siglecs have different binding preferences for sialoglycan ligands (9). While Siglec-8 has a more defined spectrum of ligands that include 6'-sulfo-sialyl Lewis x (19, 20), Siglec-9 has much broader binding spectrum of sialylated ligands (9, 21). Siglec-9 is therefore a typical PRR for Sia-SAMPs.

Recent evidence suggests that the upregulation of Sia-SAMPs can facilitate evasion of immune control during cancer progression by engaging inhibitory CD33rSiglecs such as Siglec-7 and Siglec-9 (21-26). Engagement of Siglec-7 and Siglec-9 inhibits NK cell-mediated tumor cell killing in vitro (22, 23). Siglec-9 and its murine functional paralog Siglec-E have also been implicated in myeloid cell-mediated cancer progression (21, 24). Binding of the cancer-associated sialylated glycoform of MUC1 to Siglec-9 on macrophages can induce a tumor-associated macrophage (TAM) phenotype that can promote cancer progression and immune evasion (25).

In chronic infections and cancer, expression of checkpoint molecules including PD-1, CTLA-4, TIM-3 and LAG-3 is observed on T cells and is associated with a state of T cell dysfunction termed as T cell exhaustion (27). Chronic infections such as HIV have also been shown to upregulate inhibitory CD33rSiglecs on peripheral $CD4^+$ T cells, which suggests that inhibitory Siglec receptors might be involved in T cell immunoregulation (28). In contrast, previous analyses have found very low expression of CD33rSiglecs on peripheral T cells of healthy humans (29) and mice (30). We therefore sought to characterize the Siglec expression on tumor-infiltrating T cells and to test their functional role as new potential immune-checkpoints that are regulated by glycans within the tumor microenvironment.

Results

Siglec-9 is upregulated on tumor-infiltrating T cells

We analyzed the expression of inhibitory CD33rSiglecs on immune cells in primary NSCLC samples (Supplemental Figure 1A). As previously described, CD33rSiglecs including Siglec-7 and Siglec-9 were expressed on NK cells and Siglec-9 was also expressed on myeloid cells (Supplemental Figure 1B). Several inhibitory CD33rSiglecs including Siglec-3 (CD33), Siglec-5, Siglec-7, Siglec-10 and Siglec-9 were expressed on a significant proportion of tumor-infiltrating lymphocytes (TILs) including $CD4^+$ and $CD8^+$ T cells (Figures 1A-1G and Supplemental Figures 1C-1F). Siglec-9 was the most prominently and consistently expressed CD33rSiglec on TILs across patients (Figure 1G). Lower levels of Siglec-9 were observed on peripheral blood T cells from healthy donors (Figures 1A-1C) or in spleens from patients undergoing splenectomy for non-malignant disease (Supplemental Figure 1G). There were a few healthy donors that had a larger population of Siglec-9 expressing $CD8^+$ T cells (Figure 1C). In order to further understand the heterogeneity of Siglec-9 expression, we further stained Siglec-9 on an additional and better characterized population of 49 healthy donors (Supplemental Figure 1H). The distribution of Siglec-9 on $CD8^+$ T cells was similar in both cohorts and no correlation with the age could be seen (Supplemental Figure 1I). No significant difference was seen between genders (9% in men, 7.2% in women $Sig9^+$ $CD8^+$ T cells of total CD8+ T cells). We found an inverse correlation of $Sig9^+$ $CD8^+$ with naïve $CCR7^+$ $CD45RA^+$ T cells (Supplemental Figure 1J). Immunostaining of intratumoral leukocytes showed that Siglec-9 was typically expressed on small lymphocytes and macrophages (Figure 1E). Double staining showed that Siglec-9 positive TILs in NSCLC samples also expressed CD3 (Figure 1F). We also found an upregulation of Siglec-9 on colorectal cancer (CRC) and epithelial ovarian cancer (EOC) TILs or pleural effusions (Supplemental Figure 1K).

There was a significant increase of Sia-SAMPs (Siglec-7 and Siglec-9 ligands) in lung carcinomas compared to healthy lung tissue, as well as in acute and chronic inflammatory diseases as assessed with Siglec-Fc proteins (Figure 1H and 1I). Ligands were strongly present on cytokeratin-positive cells suggesting they are in a trans-position and a trend for an increase of ligands in higher stage was observed

(Supplemental Figure 1L). As Siglec-9 was the most prominent and consistent inhibitory CD33rSiglecs upregulated on TILs across different patients, we focused our further analysis on Siglec-9.

Characterization of Siglec-9 expressing intratumoral CD8$^+$ T cells.

We aimed to further characterize the Sig9$^+$ CD8$^+$ TILs in samples from NSCLC patients by multicolor flow cytometry. Sig9$^+$ CD8$^+$ TILs co-expressed several other inhibitory receptors, including PD-1 in particular and also TIM-3 and LAG-3 (Figures 2A-2B and Supplemental Figure 2A-2D). Most Sig9$^+$ CD8$^+$ TILs were found within the population with the highest PD-1 expression (PD-1^{hi}, Supplemental Figure 2A). However, not all the PD-1^{hi} CD8$^+$ T cells expressed Siglec-9 (Supplemental Figure 2B), suggesting that Sig9$^+$ CD8$^+$ TILs are a subpopulation of tumor-specific PD-1^{hi} TILs. Sig9$^+$ CD8$^+$ T cells also expressed high levels of the transcription factor Eomesodermin (Eomes^{hi}), and low levels of T-bet (Tbet^{lo}, Supplemental Figure 2E). In general, Sig9$^+$ CD8$^+$ TILs had more inhibitory receptors upregulated and co-expressed than Sig9$^-$ CD8$^+$ TILs from NSCLC patients (Figure 2E). Several costimulatory receptors were also enriched on Sig9$^+$ CD8$^+$ TILs as compared to Sig9$^-$ CD8$^+$ TILs (Supplemental Figures 2F-2J). RNA sequencing revealed that several genes were differentially regulated between Sig9$^+$ CD8$^+$ TILs and Sig9$^-$ CD8$^+$ TILs (Supplemental Figure 2K). The three main genes upregulated in Sig9$^+$ CD8$^+$ TILs were SPP1 (osteopontin), Ki67 and KLF4 (Figure 2F). We also looked for the expression of genes involved in the generation of Sia-SAMPs. Expression of the rate-limiting enzyme for sialic acid biosynthesis, UDP-N-acetylglucosamine-2-epimerase (GNE), was higher in Sig9$^+$ CD8$^+$ TILs than in Sig9$^-$ CD8$^+$ TILs (Supplemental Figure 2L). Consequently, an upregulation of sialoglycans as shown by increased staining with SNA (Supplemental Figure 2M) and an upregulation of cis-ligands on TILs as shown by increased staining with Siglec-9-Fc protein (Supplemental Figure 2N). Protein levels of osteopontin (SPP1; Supplemental Figure 2O and 2P) and Ki-67 (Supplemental Figure 2Q) were also significantly higher in Sig9$^+$ CD8$^+$ TILs than in Sig9$^-$ CD8$^+$ TILs.

Sig9$^+$ TILs are a distinct subset within the CD8+ T cell population.

We further tested if Siglecs are upregulated by activation of T cells. While Siglec-5 expression increased significantly on polyclonally activated CD8$^+$ T cells from healthy donors, Siglec-9 was only slightly upregulated and Siglec-7 expression was unchanged (Supplemental Figure 4A). Antigen-specific stimulation of T cell clones with reactivity against peptides from influenza antigens, CMV antigens and melanA led to a slight upregulation of Siglec-9 (Supplemental Figure 4B). Sig9$^+$ CD8$^+$ TILs from NSCLC samples activated with anti-CD3/anti-CD28 antibodies expressed significantly higher surface levels of CD25 (Figure 3A), CD69 (Figure 3B) and the newly identified activation marker Siglec-5 (Supplemental Figure 4C) compared with similarly activated Sig9$^-$ CD8$^+$ TILs. Similar results were seen for polyclonally activated peripheral Sig9$^+$ CD8$^+$ cells from healthy donors (Supplemental Figures 4D-4G). CD8$^+$ T cells from NSCLC samples were clearly dysfunctional or exhausted as demonstrated by reduced production of cytokines such as IFNγ and TNFα compared with CD8$^+$ T cells from healthy donor PBMCs (Figures 3C and 3D). However, re-stimulation of TILs from NSCLC patients with anti-CD3/anti-CD28 antibodies showed that Sig9$^+$ CD8$^+$ TILs were much easier to re-stimulate and secrete at higher levels of multiple cytokines including INF-γ than Sig9$^-$ CD8$^+$ TILs (Figures 3C and 3D, Supplemental Figures 5A-5N). In addition, Sig9$^+$ CD8$^+$ cells expressed a distinct pattern of chemokine receptors including CXCR3, CXCR5, CCR4, CCR6 and CX3CR1 (Supplemental Figures 5O-5T). A recent study also found a subpopulation of PD-1^{hi} CD8$^+$ TILs with a distinct, higher functionality (31); this subpopulation was associated with an increased expression of CD5 and a lower expression of CD38 and CD101 (31). We therefore stained for these markers and found an enrichment of CD5 and Ki67 expression (Figures 3E and 3F) on Sig9$^+$ cells in the PD1^{hi} gate as well as a reduced presence of CD38$^+$ and CD101$^+$ (Figure 3G, Supplemental Figure 6). Our data provide evidence that intratumoral Sig9$^+$ CD8$^+$ cells are a distinct subpopulation of tumor-specific CD8$^+$ TILs.

Sia-SAMP-Siglec-9 interaction is a target to improve T cell activation.

Next, we wanted to explore the functional implication of Siglec expression on T cells. We used the high affinity CD33rSiglec ligand LGALS3BP that is upregulated in NSCLC

(24). LGALS3BP inhibited $CD8^+$ T cell activation in a sialic acid-dependent fashion (Figure 4A, Supplemental Figures 7A and 7B). We further generated cell lines that expressed lower surface levels of Sia-SAMPs by knocking out GNE. GNE-deficient A549 lung adenocarcinoma cells showed lower binding to Siglec-9 compared with WT A549 cells (Figure 4B). Feeding GNE-KO A549 cells with *N*-acetylneuraminic acid (Neu5Ac) to metabolically bypass the mutation led to a recovery of ligands on the cell surface and binding to Siglec-9 (Figure 4B). $CD8^+$ T cell-mediated tumor cell killing was tested by co-incubation of T cells from healthy donors and different A549 tumor cell variants in the presence of a CD3/EpCAM T cell bispecific (TCB) antibody (catumaxomab). T cell-mediated killing of GNE-KO A549 cells and desialylated A549 cells was higher compared with WT A549 cells and GNE-KO A549 cells fed with Neu5Ac (Figure 4C). Similar results were obtained with catumaxomab when using HT29 tumor cells (Supplemental Figure 7C and Figure 4D) and TILs obtained from primary NSCLC samples together with A549 and HT29 cells (Figures 4E and 4F). Experiments with the anti-CD3/CD19 TCB antibody blinatumomab and $CD19^+$ Ramos cells (Figure 4G) or primary CLL samples (Figure 4H) showed similar results. $Sig9^+$ $CD8^+$ T cells from NSCLC TILs were significantly more reactive towards GNE-KO A549 cells than $Sig9^-$ TILs, with the difference being sialic acid-dependent (Figure 4I). Similarly, $Sig9^+$ $CD8^+$ T cells induced more apoptosis in HT-29 and Ramos cells respectively than $Sig9^-$ $CD8^+$ T cells (Supplemental Figures 7E and 7F).

To test the effect of Siglec-9 blockade on T cell activation in vitro, we used a Siglec-9 antibody and the previously described Staphylococcal enterotoxin B (SEB) test (32). Two full IgG Siglec-9 antibodies (191240 and E10-286) inhibited T cell activation and therefore were agonistic (Supplemental Figures 7G and 7H). Moreover, Siglec-9 antibodies led to a dose-dependent inhibition of T cell activation tested by upregulation of the activation markers CD25 (Figure 4J) and CD69 (Supplemental Figure 7I). Addition of the Siglec-9 antibody (clone 191240) inhibited IL-2 production and CD69 expression on the surface of TILs upon SEB stimulation of primary NSCLC samples (Figures 4K and 4L). We hypothesized that bivalent binding and subsequent dimerization of Siglec-9 might be responsible for the agonistic effect on Siglec-9 by the clone 191240. Indeed, monovalent CRD-blocking Fab fragments from clone 191240

(carbohydrate recognition domain (CRD) blocking clone, Supplemental Figure 7J) significantly increased IL-2 (Figure 4K) but not CD69 (Figure 4L) production upon SEB stimulation. These findings demonstrate that T cell activation in NSCLC tumors can be increased by targeting Sia-SAMPs-Siglec-9 interactions.

Siglec-E is expressed on TILs in mice.

We further investigated if the murine functionally-equivalent paralog (Siglec-E) was upregulated on TILs in mouse models. We found a significant upregulation of Siglec-E on murine $CD8^+$ TILs when compared with splenocytes from control mice and tumor-bearing mice in the MC38 subcutaneous tumor model (Figure 5A) and other models (LLC, B16 and EMT6 subcutaneous tumor models; Supplemental Figure 8A). While other inhibitory CD33rSiglecs including Siglec-F and Siglec-G were also upregulated on the surface of murine TILs, Siglec-E was the most prominently upregulated inhibitory Siglec tested (Supplemental Figure 8B). We further analyzed the phenotype of $SigE^+$ $CD8^+$ murine TILs. The proliferation marker Ki67, the activation markers granzyme B, CD69, and the activating receptor CD27 (Figure 5B, and Supplemental Figures 8C-8E) were all significantly increased on murine $SigE^+$ $CD8^+$ TILs compared with $SigE^-$ $CD8^+$ TILs, similar to what is seen in human TIL samples. The expression and number of murine inhibitory receptors, including PD-1, was also higher on $SigE^+$ $CD8^+$ TILs than $SigE^-$ $CD8^+$ (Figures 5C-5E and Supplemental Figures 8F and 8G). $SigE^+$ $CD8^+$ TILs were predominantly terminally differentiated $Eomes^{hi}$, $Tbet^{lo}$ and $CD127^+$ T cells (Supplemental Figures 8H). Sorted murine $SigE^+$ $CD8^+$ TILs again showed a stronger re-activation than $SigE^-$ $CD8^+$ TILs, as shown by upregulation of the activation markers CD25 and CD69 (Figure 5G). Taken together, these findings suggest that $SigE^+$ $CD8^+$ TILs in mice are phenotypically similar to $Sig9^+$ $CD8^+$ TILs in humans.

Sia-SAMPs mediate immune escape in vivo.

To further investigate the role of Sia-SAMPs in immune evasion, we generated GNE-deficient MC38 cells and compared their subcutaneous growth with that of WT MC38 tumor cells. GNE-KO MC38 tumors showed a clear delay in tumor growth compared to WT MC38 tumors injected subcutaneously in C57Bl6 mice (Figure 5H). Similar

observations were made for GNE-KO and WT EMT6 tumors injected subcutaneously into BALB/c mice (Figure 5I). The GNE-KO cell lines showed no growth difference or survival in vitro (Supplemental Figure 8I). The frequencies of $CD3^+$, $CD8^+$, and $CD4^+$ T cells in leukocyte infiltrates were significantly higher in GNE-KO MC38 tumors compared with WT MC38 tumors (Figures 5J and 5K, Supplemental Figure 8J), whereas there was no difference in the infiltration of regulatory T cells (Supplemental Figure 8J). GNE-KO tumor infiltrates also contained more classical dendritic cells ($CD11c^+$ $MHCII^+$ cells within $CD45^+$ cells) than WT MC38 tumors whereas other myeloid cell types did not differ significantly (Supplemental Figure 8J). In order to analyze the role of the adaptive immunity, we repeated the experiment in mice deficient for the adaptive immune system (NOD-SCID-Gamma, NSG mice). Both MC38 and EMT6 GNE-KO cell lines showed no growth difference when compared to wildtype (WT) cell lines in NSG mice (Supplemental Figure 8K). From these findings, we concluded the sialylation directly affects tumor growth and also the anti-tumor immune response by enhancing the adaptive immune response to cancer.

Expression of Siglec receptors on T cells directly modulate anti-tumor immunity.

To further investigate the role of Sia-SAMPs and their interactions with CD33rSiglecs we used a human Siglec-9 transgenic mouse (HS9), which allows selective expression of Siglec-9 in cells producing Cre recombinase (21). Previous analysis demonstrated that human Siglec-9 binds to ligands on murine tumor cells (21). HS9 mice were crossed with CD4-Cre mice to express human Siglec-9 in T cells. These mice expressed Siglec-9 in both CD4 and CD8 T cells (Supplemental Figure 10A). The growth of syngeneic MC38 tumor cells was accelerated in mice expressing Siglec-9 in T cells and the tumors grew larger compared to littermate control mice (Figure 6A). This finding supports the hypothesis that inhibitory Siglecs on T cells can mediate immune evasion. We also used the recently developed Siglec-E16 (SigE16) transgenic mice (18). These mice express a chimeric Siglec receptor with the extracellular domain of Siglec-E and the transmembrane and intracellular domain of the activating human Siglec-16 receptor under Siglec-E promoter (18). No major differences were observed between frequency of naïve and memory T cells in different genetic animal models

(Supplemental Figure 10B). Siglec-E expression in WT and SigE16 mice was similar (Supplemental Figure 10C). Compared with WT littermate control mice, subcutaneous syngeneic MC38 tumors grew slower and remained smaller in homozygous SigE16 mice (Figure 6B). MC38 tumors had an increased induction of anti-tumor antibodies (Supplemental Figure 10D). Depletion experiments demonstrated the dependence of the effect on both $CD4^+$ and $CD8^+$ T cells and directly showed that the genetic reversal of an inhibitory into an activating Siglec receptor can also influence T cell activation (Figures 6C and 6D). We also used an adoptive transfer model to study the role of Siglec-E on T cells. We transferred OT-I T cells expressing either WT Siglec-E or activating SigE16 into WT mice with ovalbumin-expressing MC38-OVA tumors and measured the growth of tumors. MC38-OVA tumors in mice transferred with OT-I from SigE16 mice had a significantly reduced tumor growth (Figure 6E). In addition, OT-I T cells expressing SigE16 had an increased proliferation (Supplemental Figure 10E). In addition, also a trend for an increased infiltration was seen in mice adoptively transferred with SigE16 expressing OT-I T cells (Supplemental Figure 10F). To determine the effect of sialoglycans in trans-position on the growth difference in SigE16 mice, we used MC38 WT and GNE-KO cells. The previous growth difference could no longer be seen in the SigE16 background (Supplemental Figure 10G). This finding suggests that the effect seen in SigE16 mice is mediated by interactions of trans-ligands with activating SigE16 receptor.

$Sig9^+$ TILs and Siglec-9 polymorphisms are associated with clinical endpoints.

We further analyzed the correlation of Siglec expression on T cells with clinical parameters. Patients with a high frequency of $Sig9^+$ TILs (>30% of $CD8^+$ T cells) had a significantly worse overall survival (Figure 6E). The significance was slightly reduced in a multivariate analysis taking the age and also the stage into account ($p=0.0668$ with a hazard ratio of 14.6 by a Cox proportional hazard regression analysis). Recently, polymorphisms of Siglec-9 were associated with pulmonary diseases (33). We studied if the risk to develop lung cancer is associated with the rs2075803 and rs2258983 polymorphisms in the TRICL4 cohort (34). The risk to develop squamous cell lung cancer is significantly reduced in the presence of these polymorphisms (Table 1). We

also examined these polymorphisms rs2075803 and rs2258983 in 3795 cases of CRC and 3044 controls to estimate the relative risk of developing CRC. Individuals who were homozygous A for the rs2075803 SNP and homozygous C for the rs2258983 SNP had a significantly reduced risk of developing CRC (Supplemental Table 1).

Discussion

Recent studies have shown that inhibitory CD33rSiglecs can modulate the interactions of immune cells with tumor cells by sialic acid-dependent mechanisms (21-23, 25, 26), raising the possibility that these Siglecs could be used for a therapeutic checkpoint inhibition, analogous to the remarkable recent therapeutics directed against PD-1 or CTLA-4 (2). We and others have shown that T cells from healthy humans express low levels of CD33-related Siglecs (29, 35). However, we show here that expression of the inhibitory Siglec-9 is clearly increased on $CD4^+$ and $CD8^+$ TILs compared with peripheral T cells from healthy donors. We also observed the presence of Siglec ligands in both cis and trans positions. In addition, we confirmed previous observations that have shown a small population of peripheral T cells with Siglec-7 and Siglec-9 expression (35). Properly glycosylated CD52 has previously been identified as a ligand for Siglec-10 on human T cells (36). Furthermore, inhibitory mouse Siglec-G (often referred to as the murine paralog of human Siglec-10) was found to inhibit DAMP-associated T cell activation (37). These investigations demonstrate that Siglecs can dampen T cell responses in the context of general inflammation.

How Siglec-9 is upregulated on TILs and how Siglecs are regulated in T cells, including intracellular signaling, remains unclear. We observed only a slight upregulation of Siglec-9 upon polyclonal and antigen-specific stimulation of healthy T cells. Other immune checkpoint receptors are upregulated through repetitive antigenic stimulation or the tumor microenvironment including inhibitory cytokines (27). We have seen a similar effect in several mice models, indicating that the mechanism for Siglec upregulation in T cells appears to be conserved across species, even though Siglec receptors have diverged quite a lot between mice and humans. We observed a heterogeneity of the frequency in $Sig9^+$ $CD8^+$ T cells in the peripheral blood of healthy donors and an inverse correlation with the frequency of naïve $CD8^+$ T cells. This finding suggests that healthy individuals with more circulating peripheral memory T cells have also higher number of in $Sig9^+$ $CD8^+$ T cells. Until now, mainly Siglec-9 expressing NK cells and myelo-monocytic cells were associated with immune modulation in cancer. Myeloid cells were more reactive in a mouse model of Siglec-E deficiency and an increased

immunosurveillance was observed in these mice (21). Engagement of Siglec-9 on monocytes/macrophages by a cancer-associated, sialylated glycoform of MUC1 showed polarization towards immune-suppressive TAMs with upregulation of PD-L1 (25). Two analyses examined the function of inhibitory Siglec-7 and Siglec-9 in NK cell mediated tumor cell killing (22, 23). Other immune receptors including PD-1 are also expressed on myeloid cells and NK cells within the tumor (38, 39). Further experiments are needed to understand the functional relevance of these immune-modulatory receptors including Siglec-9 or PD-1 on cell types other than T cells. However, it is likely that $CD8^+$ T cells continue to play central roles in cancer immunotherapy and we define Siglec-9 on $CD8^+$ TILs as a new potential therapeutic target for cancer immunotherapy.

Further characterization of $Sig9^+$ $CD8^+$ TILs revealed that these cells co-express several inhibitory receptors including PD-1, TIM-3, Lag3 and others. Our analysis suggests that $Sig9^+$ $CD8^+$ TILs are a subpopulation of $CD8^+$ $PD\text{-}1^{hi}$ TILs, which are often tumor-specific (40). Co-expression of multiple inhibitory receptors on T cells and also $PD\text{-}1^{hi}$ TILs were associated with an exhaustion phenotype in cancer including in patients with NSCLC (27, 41). Indeed, functional analysis of TILs from NSCLC patients showed a significantly reduced capacity to produce cytokines and chemokines (Figure 3). However, $Sig9^+$ $CD8^+$ T cells from NSCLC patients were easier to re-activate than $Sig9^-$ $CD8^+$ T cell despite the increased expression of PD-1 and other inhibitory immune receptors on $Sig9^+$ TILs. This finding suggests that $Sig9^+$ $CD8^+$ TILs belong to specific subtype within the $PD\text{-}1^{hi}$ TILs. A recent analysis of chromatin states in murine and human TILs from melanoma and NSCLC patients demonstrated a subpopulation within $PD\text{-}1^{hi}$ TILs that had a relatively higher expression of CD5 and lower expression of CD38 and CD101 and that showed a greater potential for reprogrammability and reactivation (31). Our findings showed an enrichment of high CD5 expression and low CD38 and CD101 expression on $Sig9^+$ $CD8^+$ TILs in the $PD1^{hi}$ gate. This finding could be interpreted as an overlap of $Sig9^+$ $CD8^+$ TILs with this previously described tumor-specific TIL subpopulation that could be potentially re-activated by immunotherapy. Other studies have also shown that not only exhausted TILs co-express a high frequency of inhibitory receptors, but also activated TILs (42). This could mean that the

Sig9$^+$ CD8$^+$ TILs are in a higher activation state that could potentially be uncovered by blocking these different inhibitory receptors (43).

Our analysis also includes functional studies both in vitro with human tissue and in vivo in different mouse models to demonstrate the relevance of inhibitory Siglecs on TILs and their interactions with cancer-associated Sia-SAMPs. The previous studies have provided evidence that Sia-SAMP-Siglec interactions can inhibit immune cell activation in in vitro models (21-23, 25). Using bivalent anti-Siglec-9 antibodies (clones 191240 and E10-286) led to an inhibition of T cell activation and found to be agonistic, which might be due to the activation of Siglec-9 signaling by dimerization. In contrast, the use of monovalent Fab fragments of the antibody clone 191240 that inhibits Sia-SAMP-Siglec-9 interactions by hampering ligand binding to the CRD led to increased T cell activation. This result suggests that the Sia-SAMP-Siglec-9 interaction can be targeted for the enhancement of TIL activation in lung tumors. Functional relevance is further supported by the analysis of a Siglec-9 polymorphism in cancer patients. This shows an association of hypomorphic alleles with the risk of developing squamous NSCLC. In addition, the same alleles were also associated with the risk for colorectal cancer. These polymorphisms were previously associated with an increased frequency of pulmonary emphysema, exacerbations of chronic obstructive pulmonary disease and a hyperactive immune response of myeloid cells (33). While the function of these polymorphisms needs to be tested in T cells, their linkage to disease outcome suggest a role for Siglec-9 in the development of lung and colorectal cancer.

Our studies also show that the inhibitory Siglec-E receptor – the functional paralog of Siglec-9 - on murine T cells – and Sia-SAMPs in the tumor significantly influence the immune response to tumors in mouse models. Reduction of Sia-SAMPs by using GNE-KO tumor cell lines led to significantly reduced growth of tumors. In particular, the use of the more antigenic cell line EMT6-HER2 showed rejection of the tumors in some mice when hyposialylated GNE-KO tumor cells were used. The knockout of GNE in those cell lines could induce additional changes in glycosylation besides reducing the level of sialylation. An upregulation of polylactosamine could change the interaction with other

immune-modulatory lectins such as galectins (44). Also, during the growth of tumors in mice, the cells could acquire sialic acids from the host. Nevertheless, we observed a significant growth difference in two different models. Previous experiments with B16 melanoma cell lines have also shown similar results, although different approaches were used for the reduction of tumor sialylation (45). Another analysis with hyposialylated methylcholanthrene (MCA)-induced tumors has shown growth inhibition of subcutaneous tumors (46). Overexpression of inhibitory Siglec-9 on $CD4^+$ and $CD8^+$ T cells led to an increased tumor growth, which indicates a functional role of inhibitory Siglecs on T cells. Exchange of inhibitory Siglec-E with activating SigE16 (extracellular Siglec-E domain with transcellular activating human Siglec-16) showed a T cell dependent growth inhibition. In an adoptive transfer model, we demonstrated that Siglec-E on T cells is functionally involved, although the used model with ovalbumin-specific OT-I T cells has certainly limitations and ovalbumin is not directly comparable to naturally occurring tumor antigens.

Cancer immunotherapy and in particular checkpoint blockade with inhibitors of the PD-1/PD-L1/L2 axis and CTLA-4 are now routinely used in daily oncological practice (1, 47). However, only a minority of cancer patients shows objective responses under checkpoint blockade and only few develop long-term remissions. Thus, combination therapies are a promising approach to improve response rates of immunotherapies and outcomes for patients (48, 49). Our data suggest that targeting the Sia-SAMP/Siglec-9 pathway could improve anti-tumor immunity and define this pathway as new inhibitory immune checkpoint for T cell activation.

Experimental Procedures

Patients and sample preparation.

Informed consent was obtained from all patients prior to the sample collection. Surgical specimens were mechanically dissociated, digested with accutase (PAA), collagenase IV (Worthington), hyaluronidase (Sigma) and DNAse type I (Sigma), filtered, washed and frozen for future use. Single-cell suspensions were prepared. Human peripheral blood mononuclear cells (PBMCs) were isolated by density gradient centrifugation using Histopaque-1077 (Sigma) from buffy coats obtained from healthy blood donors (Blood Bank, University Hospital Basel, Switzerland). Single-cell suspensions and PBMCs were frozen for later use in liquid nitrogen.

Multicolor flow cytometry.

For multicolor flow cytometry, dead cells were stained using live/dead Fixable Blue dye (Invitrogen) and various panels of antibodies. Doublets were excluded in all analyses. Corresponding isotype antibodies or fluorescence-minus-one (FMO) samples were used as a control, in particular for the Siglec stainings. All tumor samples were analyzed with a Fortessa LSR II flow cytometer (BD Biosciences). For infiltration analysis, mice were euthanized, and tumors were mechanically dissociated and digested as described for the human sample preparation.

Staining for Siglec-7 and Siglec-9 ligands on tumor microarray.

Tissue microarrays from US Biomax were used for screening of Siglec-9 ligands expression in lung cancer samples. For the immunofluorescence staining, recombinant human Siglec-hFcs (R&D Systems) were mixed with PE-conjugated anti-human IgG (Jackson ImmunoResearch Laboratories) for 1h at 4°C prior to use. For the specific visualization of cancer cells, anti-Multi-cytokeratin (Leica Biosystems) staining was performed and visualized with a goat anti-mouse IgG coupled to Alexa Fluor 488 (Life Technologies). The general fluorescence per sample was measured in a ScanRI Microarray Scanner (Perkin Elmer) and processed with ImageJ software version 1.48 (NIH). Pictures were taken in a fluorescence microscope, original magnification X400

(Zeiss). Fluorescence was quantified using ImageJ software and normalized to background staining (secondary antibody only).

In vitro T cell activation and inhibition.

Murine and human T cells were polyclonally stimulated with anti-CD3 and anti-CD28 antibodies (BioLegend). Anti-CD3 antibodies (0.5 µg/mL) were either coated overnight at 4 °C for human T cells or added soluble for mouse T cells and anti-CD28 added at 1 µg/mL. For inhibition assays with sialylated LGALS3BP, LGALS3BP was coated overnight as well. Activation of T cells was determined by staining for activation and proliferation markers by flow cytometry or measuring cytokines in supernatants by ELISA. For the Staphylococcal enterotoxin B (SEB) assay, primary NSCLC samples were incubated at 200'000 cells/well with SEB (10 ng/mL, Sigma) for 48 hours in the presence of full length or digested Fab fragments of the 191240 anti-Siglec-9 antibody (R&D Systems). The T cell activation was assessed by FACS staining and IL-2 secretion measured in the supernatant by ELISA (BioLegend).

RNA sequencing and analysis.

CD8 positive TILs were sorted from frozen NSCLC samples by FACS according to their Siglec-9 expression. Gates used were: lymphocytes, singlets, $DAPI^-$ $CD3^+$, $CD8^+$ $CD4^-$. RNA was isolated and the library prepared by Microsynth AG (Balgach, Switzerland). Next generation sequencing of the library and data analysis was performed by Microsynth. Count data from RNAseq samples was analyzed using the edgeR Bioconductor package in R. Filtered genes, expressed at >1 count per million (cpm) in at least three samples were analyzed using the QLF functions with batch correction for patients. All genes were ranked according to their F statistics comparing Siglec-9 positive and negative samples. A weighted gene set enrichment analysis (GSEA) was performed using this pre-ranked list using the GSEA java application (http://www.broad.mit.edu/gsea/). Boxplots comparing expression levels between Siglec9 positive and negative cells was performed in R using logarithmically transformed cpm values. The dataset has been uploaded to Gene Expression Omnibus

(GEO, https://www.ncbi.nlm.nih.gov/geo, access number GSE115305).

GNE-deficient cells and in vitro tumor cell killing with CD3/EpCAM TCB or CD3/CD19 TCB.

Human and murine GNE-deficient tumor cell lines were created using CRISPR/CAS9. Guide RNAs were designed online using 'e-crisp.org', synthesized by Microsynth AG (Balgach, Switzerland) and cloned into the pX458 vector (Addgene). A549, HT-29 and RAMOS cell lines were bought from ATCC. After transient transfection in tumor cells, single cell sorting and subsequent screening for cell surface sialylation was performed. Multiple GNE-deficient clones were pooled in order to avoid clonal selection when comparing to WT cell lines.

GNE-deficient cell lines and cell lines refed with 5 mM Neu5Ac for 24h. Co-incubation with magnetically isolated CD8 T cells from healthy donors or tumor samples in the presence of catumaxomab (anti-CD3/anti-EpCAM, Fresnius) or blinatumomab, (anti-CD3/anti-CD19, Amgen) were performed at a concentration of 10 ng/ml. Alternatively, the respective cell lines were stained with CSFE (Sigma-Aldrich) and spiked into full tumor digests obtained from primary NSCLC or CRC samples. Tumor cell killing was analyzed by FACS staining for cleaved caspase 3 and by live dead staining. Tumor cells were gated by size and expression of EpCAM or CD19 respectively, as well as by negative gating using CD3, CD8 and CD4.

Genetic mouse models for in vivo analysis of Siglec function on T cells.

Siglec-9 transgenic mice were described previously (21). Siglec-9 transgenic mice (B6.Cg-Tg(CAG-Siglec9)1Avrk) were crossed with CD4-Cre mice (B6Tg(CD4-cre)1Cwi) to obtain a T cell specific overexpression of inhibitory human Siglec-9 in the C57Bl6 background. Transgenic mice expressing SigE16 chimeric Siglec-E with transmembrane and intracellular domain of activating human Siglec-16 (B6.Cg-Siglece<tm4E16Avrk>) were also described previously (18). Tumor cell lines were injected into 8 to 12-week old female mice, and tumor growth monitored as described above.

SigE16 were crossed into OT-I transgenic mice. For the adoptive transfer of ovalbumin-specific OT-I cells from WT or SigE16 mice, T cells were harvested from splenocytes and injected into WT C57Bl6 mice bearing subcutaneous MC38-OVA tumors. T cells were followed for proliferation by labeling with Cell Trace Violet (CTV). Tumor growth was measured, and cell numbers determined by counting beads and flow cytometry.

Association study of Siglec-9 polymorphism

The association analysis of Siglec-9 polymorphisms in lung cancer was studied on the TRILC cohort (34). In total, 11348 patients with lung cancer and 15861 controls were studied for the rs2075803 and the rs2258983 SNP. An association test was performed after adjusting for age, gender, and top significant principal components. Then, we conducted a fixed effects meta-analysis with an inverse variance-weighted average method to combine the summary data from each association test. Meta-analysis was performed using SAS version 9.4 (SAS Institute Inc., Cary, NC, USA). For the analysis of an association of Siglec-9 polymorphisms with the risk of colorectal cancer, SNP genotypes for rs2075803, rs2258983 among cases and controls from imputed genotype data derived from samples genotyped on the Oncoarray platform and USC Norris Cancer Center were used (informed consent was obtained from all patients). Using contingency table analysis (Fisher's test), we calculated odds ratios, 95% confidence intervals and p-values using an additive model, and genotype-specific odds ratios.

Statistical analysis

Statistical significance between two groups was determined using two tailed Student's t tests. Significance between more than two conditions was assessed using one-way ANOVAs with multiple comparisons. For survival curve analysis, two-way ANOVA was used. Survival analysis was performed by the Gehan-Breslow-Wilcoxon test and multivariate analysis was done by Cox proportional hazard analysis. A P value <0.05 was considered statistically significant.

Study approval

The local ethical committee in Basel, Switzerland approved the sample collection and the use of clinical data (Ethikkomission Nordwest- und Zentralschweiz, EK321/10 and UBE 15–106). Mouse experiments were approved by the local committee of Basel Stadt (approval number 2747).

Acknowledgments

This work was supported by funding from the Goldschmidt-Jacobson Foundation (to H.L.), the Promedica Foundation (to M.S. and A.Z.), Krebsliga Beider Basel (KLBB, to H.L.), Lichtenstein Foundation (to H.L.), Schoenmakers Foundation (to H.L.), Huggenberger Foundation (to H.L), NIH (to A.V., P01 HL107150). We thank Patrick Secrest, Petra Herzig and Béatrice Dolder-Schlienger for their technical assistance. We thank Pedro Romero, Camilla Jandus and Marc Donath for critically reading the manuscript. We also thank all the patients that allowed us to use their material and made this work possible.

Author contributions

M.S., S.S.S. planned and conducted the experiments and analyzed the data. H.L. conceived idea and planned the project. M.S., D.E.S., A.V., A.Z. and H.L. wrote the manuscript. M.P.T., D.T. K.F.B., S.V.G., A.T., F.S. performed experiments. L.T., D.L., V.H., M.V.B., A.E., M.S. provided important material for the research. W.Z., H.J.L., Y.H., C.A. analyzed the Siglec polymorphisms.

Declaration of interests

There is no conflict of interest of any of the authors.

References

1. Topalian SL, Drake CG, and Pardoll DM. Immune checkpoint blockade: a common denominator approach to cancer therapy. *Cancer Cell.* 2015;27(4):450-61.
2. Chen DS, and Mellman I. Elements of cancer immunity and the cancer-immune set point. *Nature.* 2017;541(7637):321-30.
3. Cao X. Self-regulation and cross-regulation of pattern-recognition receptor signalling in health and disease. *Nat Rev Immunol.* 2016;16(1):35-50.
4. Schaefer L. Complexity of danger: the diverse nature of damage-associated molecular patterns. *J Biol Chem.* 2014;289(51):35237-45.
5. Mogensen TH. Pathogen recognition and inflammatory signaling in innate immune defenses. *Clin Microbiol Rev.* 2009;22(2):240-73, Table of Contents.
6. Chen GY, and Nunez G. Sterile inflammation: sensing and reacting to damage. *Nat Rev Immunol.* 2010;10(12):826-37.
7. Wang RF, Miyahara Y, and Wang HY. Toll-like receptors and immune regulation: implications for cancer therapy. *Oncogene.* 2008;27(2):181-9.
8. Varki A. Since there are PAMPs and DAMPs, there must be SAMPs? Glycan "self-associated molecular patterns" dampen innate immunity, but pathogens can mimic them. *Glycobiology.* 2011;21(9):1121-4.
9. Padler-Karavani V, Hurtado-Ziola N, Chang YC, Sonnenburg JL, Ronaghy A, Yu H, et al. Rapid evolution of binding specificities and expression patterns of inhibitory CD33-related Siglecs in primates. *FASEB J.* 2014;28(3):1280-93.
10. Crocker PR, Paulson JC, and Varki A. Siglecs and their roles in the immune system. *Nat Rev Immunol.* 2007;7(4):255-66.
11. Macauley MS, Crocker PR, and Paulson JC. Siglec-mediated regulation of immune cell function in disease. *Nat Rev Immunol.* 2014;14(10):653-66.
12. Pearce OM, and Laubli H. Sialic acids in cancer biology and immunity. *Glycobiology.* 2015.
13. Nitschke L. CD22 and Siglec-G regulate inhibition of B-cell signaling by sialic acid ligand binding and control B-cell tolerance. *Glycobiology.* 2014;24(9):807-17.
14. Chang YC, and Nizet V. The interplay between Siglecs and sialylated pathogens. *Glycobiology.* 2014;24(9):818-25.
15. Chang YC, Olson J, Beasley FC, Tung C, Zhang J, Crocker PR, et al. Group B Streptococcus engages an inhibitory Siglec through sialic acid mimicry to blunt innate immune and inflammatory responses in vivo. *PLoS Pathog.* 2014;10(1):e1003846.
16. Carlin AF, Chang YC, Areschoug T, Lindahl G, Hurtado-Ziola N, King CC, et al. Group B Streptococcus suppression of phagocyte functions by protein-mediated engagement of human Siglec-5. *J Exp Med.* 2009;206(8):1691-9.
17. Carlin AF, Uchiyama S, Chang YC, Lewis AL, Nizet V, and Varki A. Molecular mimicry of host sialylated glycans allows a bacterial pathogen to engage neutrophil Siglec-9 and dampen the innate immune response. *Blood.* 2009;113(14):3333-6.

18. Schwarz F, Landig CS, Siddiqui S, Secundino I, Olson J, Varki N, et al. Paired Siglec receptors generate opposite inflammatory responses to a human-specific pathogen. *EMBO J.* 2017.
19. Propster JM, Yang F, Rabbani S, Ernst B, Allain FH, and Schubert M. Structural basis for sulfation-dependent self-glycan recognition by the human immune-inhibitory receptor Siglec-8. *Proc Natl Acad Sci U S A.* 2016;113(29):E4170-9.
20. Yu H, Gonzalez-Gil A, Wei Y, Fernandes SM, Porell RN, Vajn K, et al. Siglec-8 and Siglec-9 binding specificities and endogenous airway ligand distributions and properties. *Glycobiology.* 2017;27(7):657-68.
21. Laubli H, Pearce OM, Schwarz F, Siddiqui SS, Deng L, Stanczak MA, et al. Engagement of myelomonocytic Siglecs by tumor-associated ligands modulates the innate immune response to cancer. *Proc Natl Acad Sci U S A.* 2014;111(39):14211-6.
22. Jandus C, Boligan KF, Chijioke O, Liu H, Dahlhaus M, Demoulins T, et al. Interactions between Siglec-7/9 receptors and ligands influence NK cell-dependent tumor immunosurveillance. *J Clin Invest.* 2014;124(4):1810-20.
23. Hudak JE, Canham SM, and Bertozzi CR. Glycocalyx engineering reveals a Siglec-based mechanism for NK cell immunoevasion. *Nat Chem Biol.* 2014;10(1):69-75.
24. Laubli H, Alisson-Silva F, Stanczak MA, Siddiqui SS, Deng L, Verhagen A, et al. Lectin galactoside-binding soluble 3 binding protein (LGALS3BP) is a tumor-associated immunomodulatory ligand for CD33-related Siglecs. *J Biol Chem.* 2014;289(48):33481-91.
25. Beatson R, Tajadura-Ortega V, Achkova D, Picco G, Tsourouktsoglou TD, Klausing S, et al. The mucin MUC1 modulates the tumor immunological microenvironment through engagement of the lectin Siglec-9. *Nat Immunol.* 2016.
26. RodrIguez E, Schetters STT, and van Kooyk Y. The tumour glyco-code as a novel immune checkpoint for immunotherapy. *Nat Rev Immunol.* 2018;18(3):204-11.
27. Wherry EJ, and Kurachi M. Molecular and cellular insights into T cell exhaustion. *Nat Rev Immunol.* 2015;15(8):486-99.
28. Soto PC, Karris MY, Spina CA, Richman DD, and Varki A. Cell-intrinsic mechanism involving Siglec-5 associated with divergent outcomes of HIV-1 infection in human and chimpanzee CD4 T cells. *J Mol Med (Berl).* 2013;91(2):261-70.
29. Nguyen DH, Hurtado-Ziola N, Gagneux P, and Varki A. Loss of Siglec expression on T lymphocytes during human evolution. *Proc Natl Acad Sci U S A.* 2006;103(20):7765-70.
30. Crocker PR, McMillan SJ, and Richards HE. CD33-related siglecs as potential modulators of inflammatory responses. *Ann N Y Acad Sci.* 2012;1253:102-11.
31. Philip M, Fairchild L, Sun L, Horste EL, Camara S, Shakiba M, et al. Chromatin states define tumour-specific T cell dysfunction and reprogramming. *Nature.* 2017;545(7655):452-6.

32. Wang C, Thudium KB, Han M, Wang XT, Huang H, Feingersh D, et al. In vitro characterization of the anti-PD-1 antibody nivolumab, BMS-936558, and in vivo toxicology in non-human primates. *Cancer Immunol Res.* 2014;2(9):846-56.
33. Ishii T, Angata T, Wan ES, Cho MH, Motegi T, Gao C, et al. Influence of SIGLEC9 polymorphisms on COPD phenotypes including exacerbation frequency. *Respirology.* 2016.
34. Wang Y, McKay JD, Rafnar T, Wang Z, Timofeeva MN, Broderick P, et al. Rare variants of large effect in BRCA2 and CHEK2 affect risk of lung cancer. *Nat Genet.* 2014;46(7):736-41.
35. Ikehara Y, Ikehara SK, and Paulson JC. Negative regulation of T cell receptor signaling by Siglec-7 (p70/AIRM) and Siglec-9. *J Biol Chem.* 2004;279(41):43117-25.
36. Bandala-Sanchez E, Zhang Y, Reinwald S, Dromey JA, Lee BH, Qian J, et al. T cell regulation mediated by interaction of soluble CD52 with the inhibitory receptor Siglec-10. *Nat Immunol.* 2013;14(7):741-8.
37. Toubai T, Rossi C, Oravecz-Wilson K, Zajac C, Liu C, Braun T, et al. Siglec-G represses DAMP-mediated effects on T cells. *JCI Insight.* 2017;2(14).
38. Gordon SR, Maute RL, Dulken BW, Hutter G, George BM, McCracken MN, et al. PD-1 expression by tumour-associated macrophages inhibits phagocytosis and tumour immunity. *Nature.* 2017;545(7655):495-9.
39. Liu Y, Cheng Y, Xu Y, Wang Z, Du X, Li C, et al. Increased expression of programmed cell death protein 1 on NK cells inhibits NK-cell-mediated anti-tumor function and indicates poor prognosis in digestive cancers. *Oncogene.* 2017.
40. Gros A, Robbins PF, Yao X, Li YF, Turcotte S, Tran E, et al. PD-1 identifies the patient-specific CD8(+) tumor-reactive repertoire infiltrating human tumors. *J Clin Invest.* 2014;124(5):2246-59.
41. Thommen DS, Schreiner J, Muller P, Herzig P, Roller A, Belousov A, et al. Progression of Lung Cancer Is Associated with Increased Dysfunction of T Cells Defined by Coexpression of Multiple Inhibitory Receptors. *Cancer Immunol Res.* 2015;3(12):1344-55.
42. Legat A, Speiser DE, Pircher H, Zehn D, and Fuertes Marraco SA. Inhibitory Receptor Expression Depends More Dominantly on Differentiation and Activation than "Exhaustion" of Human CD8 T Cells. *Front Immunol.* 2013;4:455.
43. Speiser DE, Ho PC, and Verdeil G. Regulatory circuits of T cell function in cancer. *Nat Rev Immunol.* 2016;16(10):599-611.
44. Rabinovich GA, and Croci DO. Regulatory circuits mediated by lectin-glycan interactions in autoimmunity and cancer. *Immunity.* 2012;36(3):322-35.
45. Perdicchio M, Cornelissen LA, Streng-Ouwehand I, Engels S, Verstege MI, Boon L, et al. Tumor sialylation impedes T cell mediated anti-tumor responses while promoting tumor associated-regulatory T cells. *Oncotarget.* 2016;7(8):8771-82.
46. Cohen M, Elkabets M, Perlmutter M, Porgador A, Voronov E, Apte RN, et al. Sialylation of 3-methylcholanthrene-induced fibrosarcoma determines antitumor immune responses during immunoediting. *J Immunol.* 2010;185(10):5869-78.
47. Sharma P, and Allison JP. The future of immune checkpoint therapy. *Science.* 2015;348(6230):56-61.

48. Sharma P, and Allison JP. Immune checkpoint targeting in cancer therapy: toward combination strategies with curative potential. *Cell.* 2015;161(2):205-14.
49. Melero I, Berman DM, Aznar MA, Korman AJ, Perez Gracia JL, and Haanen J. Evolving synergistic combinations of targeted immunotherapies to combat cancer. *Nat Rev Cancer.* 2015;15(8):457-72.

Figure Legends

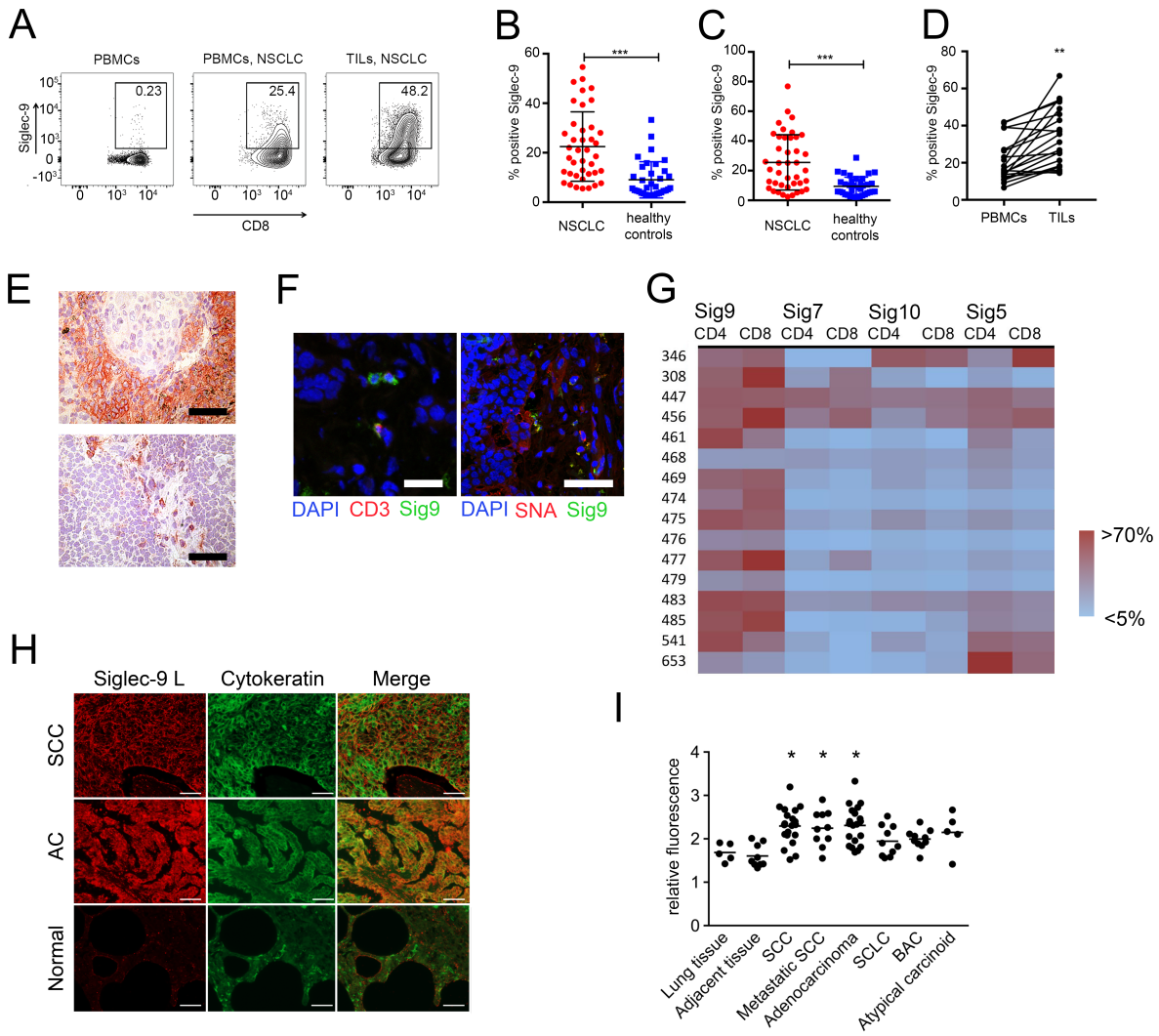

Figure 1 Siglec-9 is upregulated on CD8$^+$ TILs.

(**A**) Representative flow cytometry analysis of Siglec-9 expression on CD8$^+$ T cells in PBMCs from healthy donors (left panel), PBMCs from NSCLC patients (middle panel) and TILs from a matched NSCLC patient (right panel). (**B**, **C**), Quantification of Siglec-9 expression on CD4$^+$ (B) and CD8$^+$ (C) TILs from NSCLC patients (PBMCs *n*=36, NSCLC *n*=41, mean±s.d.). Statistical analysis by unpaired Student's t test. (**D**) Paired analysis of CD8$^+$ T cells from the peripheral blood and tumors of NSCLC patients (*n*=20). Statistical analysis by paired Student's t test. (**E**) Immunohistochemical staining of Siglec-9 positive cells in NSCLC sections. Scale bars represent 50 μm. (**F**) Representative immunofluorescence analysis of CD3 and Siglec-9 double positive cells

(left panel; arrow shows double positive cell; scale bar=30 μm) and Siglec-9 staining or SNA staining and Siglec-9 staining (right panel, scale bar=50 μm). (**G**) Heatmap of expression analysis of different Siglecs in NSCLC samples on $CD4^+$ and $CD8^+$ TILs. and (**H**, **I**) Immunofluorescence study in paraffin-embedded tissue microarrays using recombinant Siglec-9-Fc (human IgG1) fusion protein coupled to secondary PE-conjugated (Fab′)2 goat anti-human Fc antibody. Representative images (H) and Siglec ligands quantification summary (I) are shown. The pictures were taken with an original magnification x400, the scale bars represent 50μm. Fluorescence values were normalized against an IgG1 isotype control (lung tissue *n*=5, adjacent lung tissue *n*=9, squamous cell carcinoma SCC *n*=20, adenocarcinoma *n*=20, small cell lung cancer SCLC *n*=10, broncho-alveolar carcinoma BAC *n*=10, atypical carcinoid *n*=5, mean ±s.e.m.). Statistical analysis was performed by 1-way-ANOVA. **P*<0.05, ***P*<0.01, ****P*<0.001.

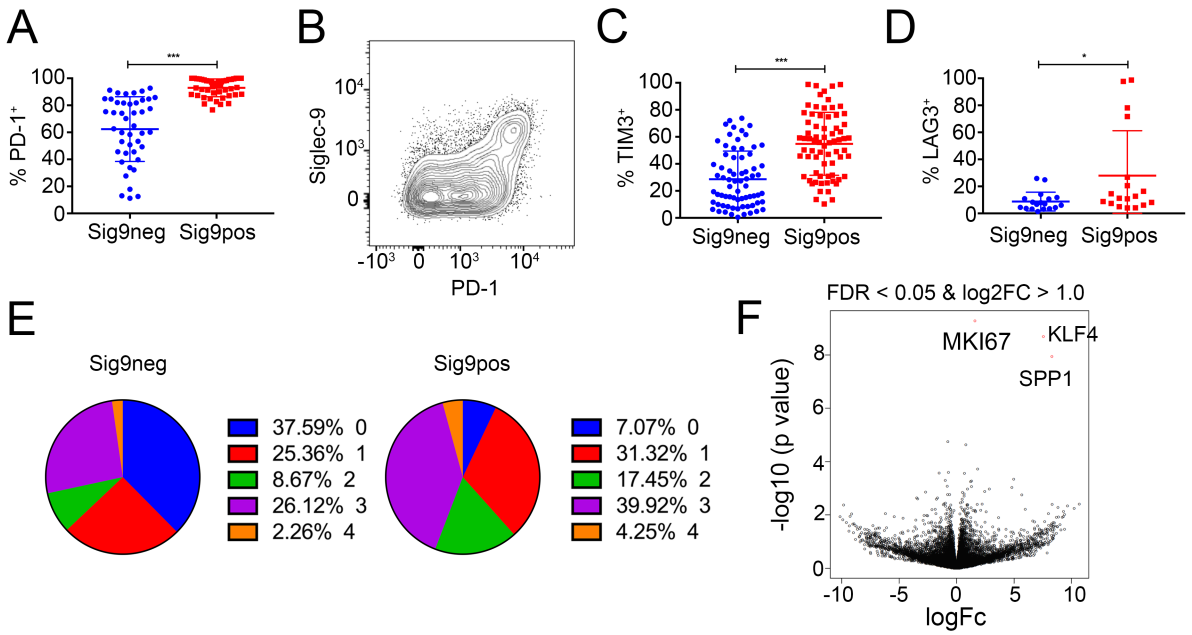

Figure 2 Sig9^{+} CD8^{+} TILs co-express inhibitory receptors.

(**A**, **B**) Expression of PD-1 in primary NSCLC samples on Sig9^{-} CD8^{+} or Sig9^{+} CD8^{+} TILs (A, *n*=44) and representative FACS analysis (B). Statistical analysis by paired Student's t test. (**C**, **D**) Expression of TIM-3 (C, *n*=71) and LAG-3 (D, *n*=18) on Sig9^{-} CD8^{+} or Sig9^{+} CD8^{+} TILs from NSCLC samples. Statistical analysis by paired Student's t test. (**E**) Analysis of the number of co-expressed inhibitory receptors on Sig9^{-} CD8^{+} or Sig9^{+} CD8^{+} TILs. (**F**) Volcano plot of RNA sequencing on sorted TILs according to their Siglec-9 expression. The three significantly differentially expressed genes were MIK67 (Ki67), KLF4 and SPP1. *P<0.05, ***P<0.001. Data presented as mean±s.d.

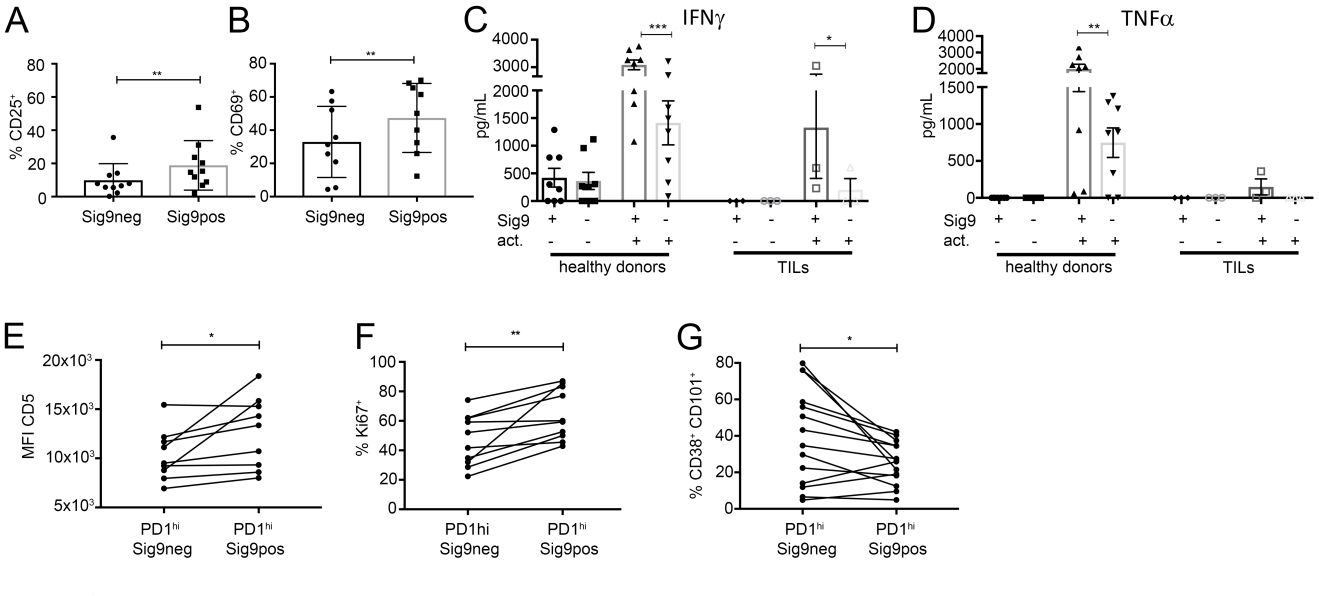

Figure 3 Sig9$^+$ CD8$^+$ TILs are a distinct subset within intratumoral CD8$^+$ T cells.

(**A**, **B**) Upregulation of the activation marker CD25 (A) and CD69 (B) on Sig9$^-$ CD8$^+$ or Sig9$^+$ TILs sorted from primary NSCLC samples and activated with anti-CD3/28 antibodies for 48h (*n*=9). Statistical analysis by paired Student's t test. (**C**) ELISA analysis of IFNγ in the supernatant of sorted Sig9$^-$ CD8$^+$ T cells or Sig9$^+$ CD8$^+$ T cells (*n*=3-7, independent patients). Cells were sorted from PBMCs of healthy donors (HD) or primary NSCLC samples (TILs). Supernatants from 50'000 cells were analyzed. (**D**) Analysis of TNFα in the supernatant of sorted Sig9$^-$ CD8$^+$ or Sig9$^+$ CD8$^+$ cells from healthy donors or NSCLC patient samples (*n*=3-7, independent donors/patients). Statistical analysis was performed by 1-way-ANOVA. (**E**) Expression level of CD5 in the CD8$^+$ PD1^{hi} population on Sig9$^-$ TILs and Sig9$^+$ TILs (*n*=9). (**F**) Percent of Sig9$^-$ CD8$^+$ TILs or Sig9$^+$ CD8$^+$ TILs in primary NSCLC samples that express Ki67 within the PD1^{hi} population (*n*=9). (**G**) Frequency of CD38^{hi} CD101^{hi} cells on Sig9$^-$ and Sig9$^+$ CD8$^+$ PD1^{hi} TILs determined by flow cytometric analysis (*n*=13). Statistical analysis by paired Student's t test. *P<0.05, **P<0.01, ***P<0.001. Data presented as mean±s.d.

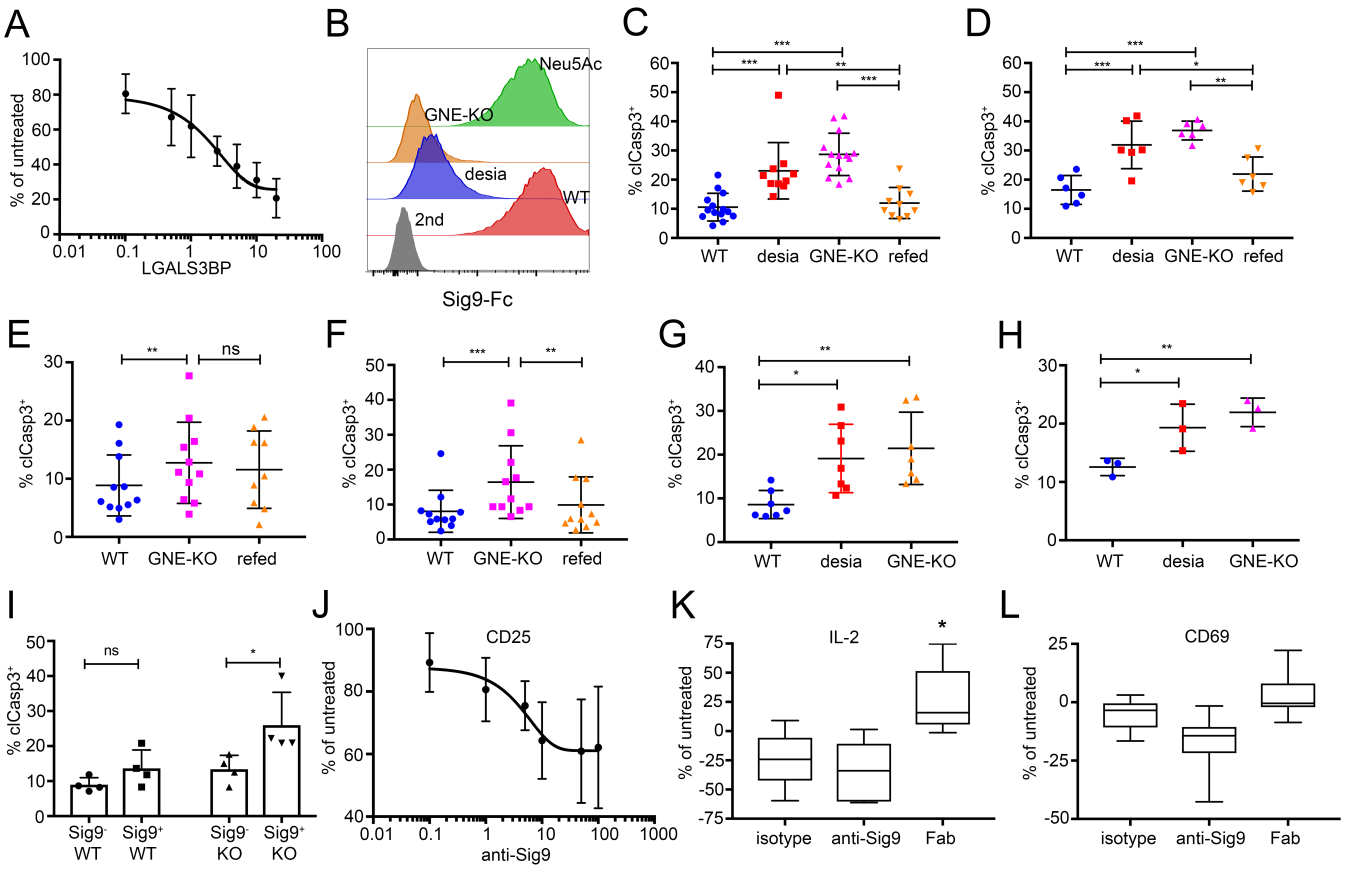

Figure 4 Sialoglycan-SAMPs inhibit T cell-mediated tumor cell killing in vitro.

(**A**) Inhibition of T cell activation by LGALS3BP in a dose-dependent manner measured by intracellular IFNγ by flow cytometry. $CD8^+$ T cells from healthy donors were activated with anti-CD3 and anti-CD28 antibodies in presence of increasing amounts of LGALS3BP (μg/mL, *n*=3). (**B**) Representative histograms of binding of Sig9-Fc to A549 WT cells, enzymatically desialylated A549 cells (desia), GNE-deficient A549 cells (GNE-KO) and GNE-KO A549 cells refed with 10 mM Neu5Ac. (**C**) Percentage of cleaved caspase 3 positive ($clCasp3^+$) WT A549 cells, desialylated A549 cells, GNE-KO A549 cells or GNE-KO A549 cells fed with Neu5Ac (refed) after incubation with $CD8^+$ T cells and catumaxomab (*n*=10). (**D**) Apoptosis of WT, desialylated, GNE-KO and refed GNE-KO HT-29 cells measured by upregulation of cleaved caspase 3 in tumor cells (*n*=6). (**E**, **F**) $clCaps3^+$ A549 (E, *n*=11) or HT-29 (F, *n*=11) tumor cells after co-incubation with TILs from NSCLC or CRC samples. (**G**) $CD8^+$ T cells were sorted according to their Siglec-9 expression and incubated with either WT or GNE-KO A549 cells (*n*=4). (**H**) $CD19^+$ RAMOS cells were incubated with $CD8^+$ T cells from healthy donors in the presence of

CD3 and CD19 bispecific antibody blinatumomab (*n*=7). (**I**) GNE-KO RAMOS cells incubated with $CD8^+$ T cells from patients with chronic lymphocytic leukemia (*n*=3). (**J**) Activation measured by CD25 on $CD8^+$ T cells treated with anti-CD3 and anti-CD28 antibodies in presence of anti-Siglec-9 antibody (clone 191240, μg/mL, *n*=4). (**K**) Relative IL-2 production of NSCLC primary tumor samples incubated with SEB and Siglec-9 blocking antibody and the Fab fragments (clone 191240, *n*=5). (**L**) Measurement of CD69 upregulation on $CD8^+$ TILs from NSCLC patients upon incubation with SEB in presence of antibodies or Fab fragments (*n*=5). Statistical analyses in this figure were performed by 1-way-ANOVA. Data presented as mean±s.d. **P*<0.05, ***P*<0.01, ****P*<0.001.

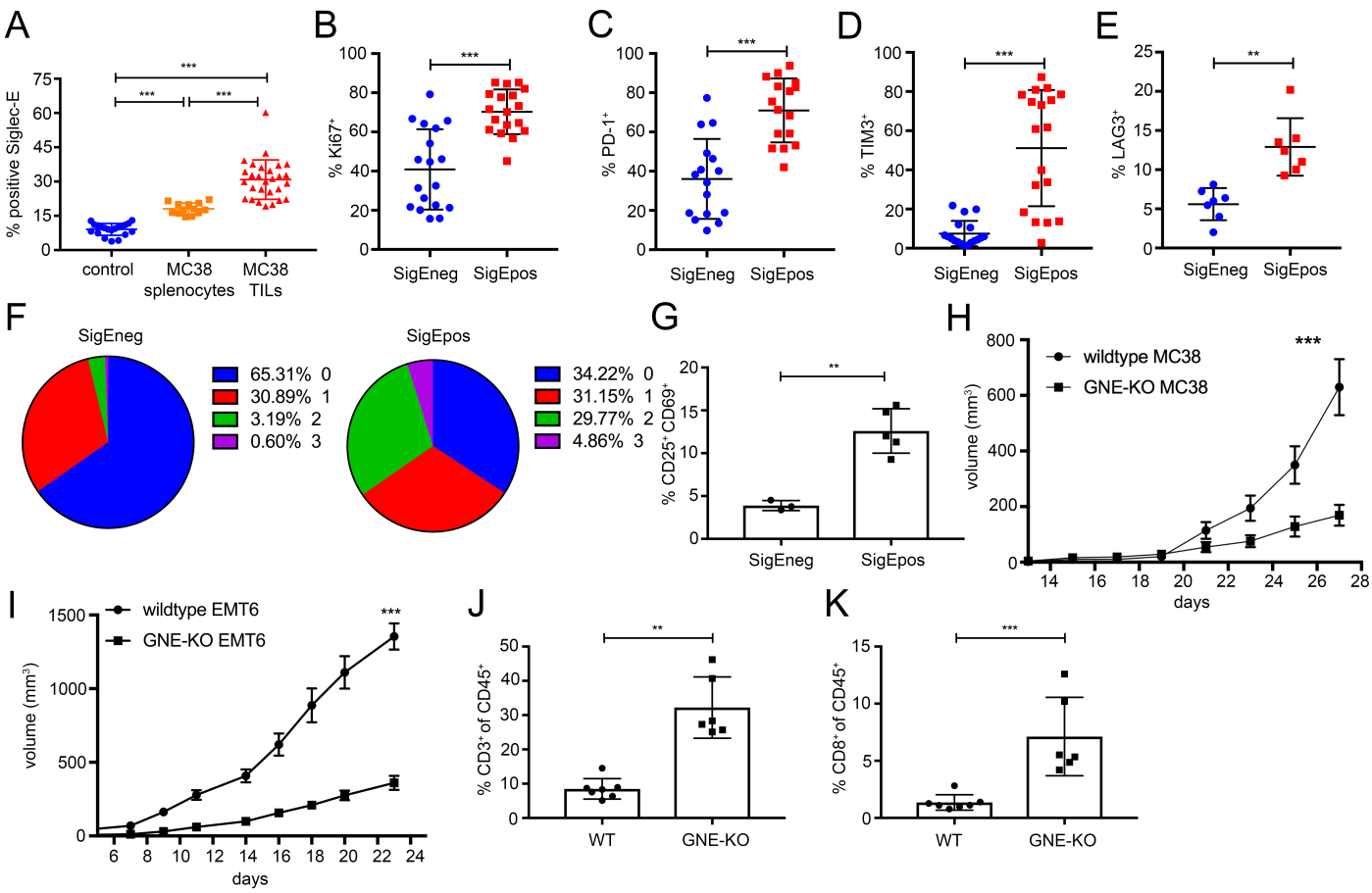

Figure 5 Sialylated-SAMPs enhance immune escape and tumor growth in vivo.

(**A**) Siglec-E expression was determined by flow cytometry on control (ctrl) splenocytes, splenocytes from tumor-bearing mice and $CD8^+$ TILs from subcutaneous MC38 tumors (*n*=25-28). Statistical analysis was performed by 1-way-ANOVA. (**B**) Expression of intracellular Ki67, was examined by flow cytometry on $SigE^-$ $CD8^+$ and $SigE^+$ $CD8^+$ TILs (*n*=18). Statistical analysis by paired Student's t test. (**C-E**) Frequencies of inhibitory immune receptor expression on $SigE^-$ $CD8^+$ and $SigE^+$ $CD8^+$ TILs from MC38 tumors as studied by flow cytometry PD-1 (C, *n*=16), TIM-3 (D, *n*=18), and LAG-3 (E, *n*=7) were analyzed. Statistical analysis by paired Student's t test. (**F**) Number of co-expressed inhibitory receptors on $SigE^-$ $CD8^+$ or $SigE^+$ $CD8^+$ TILs. (**G**) Upregulation of $CD25^+$ $CD69^+$ upon re-stimulation of sorted $SigE^-$ $CD8^+$ and $SigE^+$ $CD8^+$ TILs. Statistical analysis by paired Student's t test. (**H**) Growth curves of subcutaneous WT or GNE-deficient (GNE-KO) MC38 tumors (*n*=8-9). (**I**) Growth curves of subcutaneous WT and

GNE-KO EMT6 tumors (*n*=13-14). Experiments were replicated 2-3 times. Statistical analysis by 2-way-ANOVA. (**J**, **K**) Frequencies of $CD3^+$ and $CD8^+$ cells in the tumor (*n*=7). Statistical analysis by unpaired Student's t test. ***P*<0.01, ****P*<0.001. Data presented as mean±s.d.

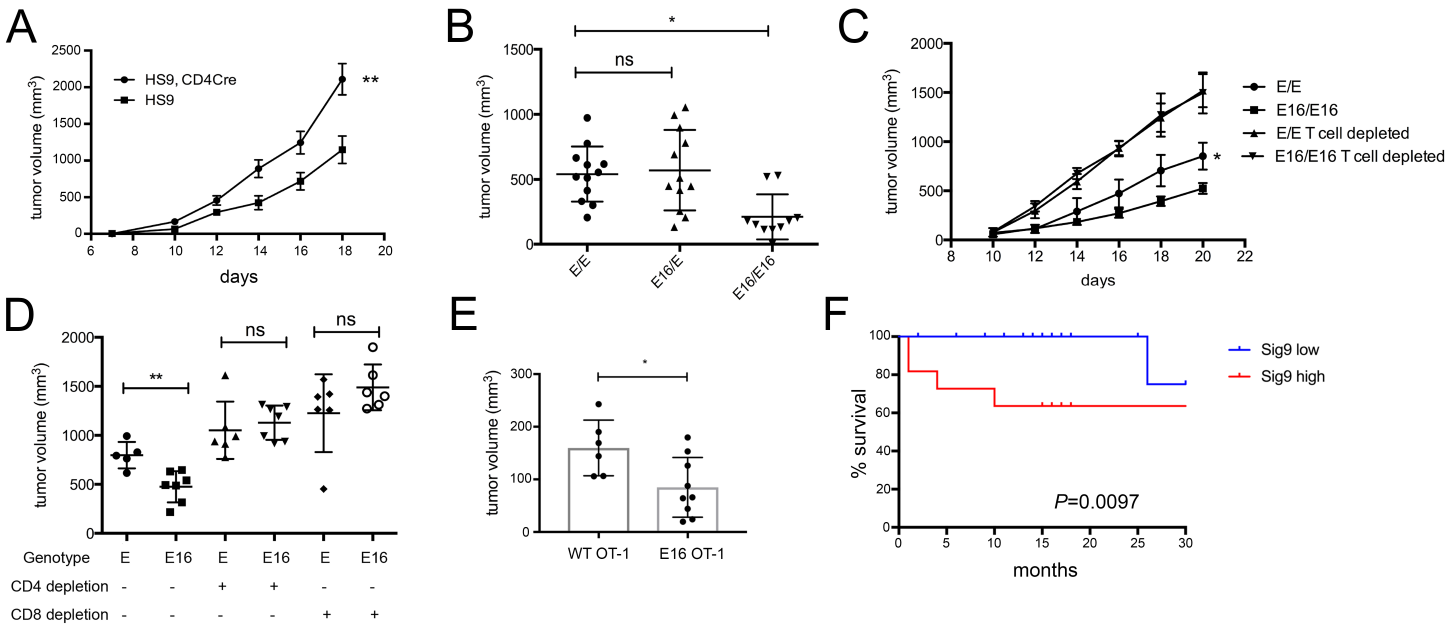

Figure 6 Engagement of inhibitory Siglecs on T cells mediates immune escape.

(**A**) Subcutaneous growth curves of MC38 tumors in littermate Siglec-9 transgenic control mice (HS9) or Siglec-9 transgenic mice crossed to CD4-Cre mice (HS9, CD4Cre) (*n*=8-10). The experiment was repeated 3 times. Statistical analysis by 2-way-ANOVA. (**B**) Tumor volumes after 21 days of subcutaneous MC38 tumors in littermate control mice (E/E), or homozygous (E16/E16) mice that express the chimeric receptor SigE16 (*n*=7). Statistical analysis was performed by 1-way-ANOVA. (**C**) Subcutaneous growth curves of MC38 tumors in E16 mice or littermate control mice after CD4 and CD8 cell depletion by antibodies (*n*=7-8). The experiment was repeated 2 times. Statistical analysis by 2-way-ANOVA. (**D**) MC38 tumor volumes after 21 days in E16 mice and littermate control mice and independent depletion of CD4 and CD8 T cells. (**E**) Tumor volume of MC38-OVA tumors after adoptive transfer of ovalbumin-specific OT-I $CD8^+$ T cells from WT or SigE16 (E16) mice. Statistical analysis was performed by 1-way-ANOVA. **P*<0.05, ***P*<0.01. Data presented as mean±s.d. (**F**) Survival analysis of NSCLC patients with low (*n*=18) and high percentage (above 30%, *n*=11) of Siglec-9 expression on their $CD8^+$ T cells. Differences were analyzed by the Wilcoxon test. A multivariate analysis of the two groups for age and stage show a slightly reduced

significance with a *P* value of 0.0669 (multivariate, univariate analysis *P*=0.0097) and a hazard ratio of 14.6.

Table 1 Risk for lung cancer depending on Siglec-9 polymorphisms

	rs_number	reference allele	effect allele	OR	95%CI_l	95%CI_u	*P* value
NSCLC	rs2075803	A	G	0.998	0.963	1.035	0.92
NSCLC	rs2258983	C	A	0.998	0.962	1.035	0.91
Adenocarcinoma	rs2075803	A	G	1.03	0.974	1.09	0.29
Adenocarcinoma	rs2258983	C	A	1.036	0.978	1.097	0.23
Squamous	rs2075803	A	G	0.939	0.888	0.993	0.027
Squamous	rs2258983	C	A	0.936	0.884	0.991	0.023

OR, odds ratio; 95%CI_l, 95% lower confidence interval; 95%CI_u, 95% upper confidence interval; *P* value by Cox proportional regression analysis, multivariate analysis for age, gender and top significant principal components form previous studies.